Radar Signal Recognition Based on Dual-Channel Model With HOG Feature Extraction

Zeyu Tang, Daying Quan, *Member, IEEE*, Xiaofeng Wang, Ning Jin, and Dongping Zhang

***Abstract*—*Objectives:* To improve the recognition accuracy of radar signals under a low signal-to-noise ratio (SNR). *Technology or Method:* We propose a novel radar signal recognition method based on a dual-channel model with the histogram of oriented gradients (HOG) feature extraction. Specifically, multisynchrosqueezing transform (MSST) and Choi–Williams distribution (CWD) transform are adopted individually to obtain the time–frequency distribution images of radar signals, and HOG feature extraction is performed on the preprocessed time–frequency images of each channel, respectively. Then, the features of the two channels are fused and dimensionally reduced by the principal component analysis (PCA). Finally, the compact feature parameters are fed to the support vector machine (SVM) classifier to identify radar signals. *Clinical or Biological Impact:* The experimental results demonstrate that the proposed model achieves a high recognition performance with a small computational complexity, especially in low SNR. When the SNR is −12 dB, the recognition accuracy can reach more than 92%, which is over 6% higher than that of single-channel models and related convolutional neural network-based models.**

***Index Terms*—Choi–Williams distribution (CWD) time–frequency analysis (TFA), histogram of oriented gradient (HOG), low probability of intercept (LPI) radar signal, multisynchrosqueezing transform (MSST), signal recognition.**

I. Introduction

ELECTRONIC reconnaissance provides a powerful guarantee for defense and attack on the battlefield by intercepting enemy electromagnetic signals and estimating signal parameters [1], while the low probability of intercept (LPI) radar signal recognition is a major concern in electronic reconnaissance [2], [3]. Effective identification of LPI radar signals can help us to gain initiative on the battlefield, and then influence further operational decisions [4]. Conventional radar signal recognition mainly relies on pulse description words, such as carrier frequency, pulse width, pulse amplitude, arrival time, and arrival angle [5]. Such recognition techniques based on intersignal parameters can achieve satisfying results in the case of low signal flow density, simple signal form, a small number of radiation sources, and a simple electromagnetic environment. However, with the advancement of radar technologies and the introduction of LPI radars, the electronic countermeasure environment becomes increasingly complex. LPI radars are characterized by low interception, high detection, large time width, and strong interference, which brings great challenges to radar signal recognition.

In recent years, lots of work have focused on radar signal recognition by analyzing the characteristics of radar signals in the time domain, frequency domain, and time–frequency domain [6]. For the time domain, Mingqiu et al. [7] used high-order statistics and wavelet ridge to extract signal features for recognition. Iglesias et al. [2] distinguished signal types by calculating various signal characteristics, such as frequency peak and variance based on instantaneous phase and normalized instantaneous frequency of signals. Wang et al. [8] calculated four features, including the variance and the entropy of the autocorrelation functions, and the maximum values and the entropy of the power spectrums, and used the directed graph model to characterize the joint probability distribution of features and categories. For the frequency domain, Wei et al. [9] proposed a hybrid neural network model which includes shallow convolutional neural network (CNN), long- and short-term memory (LSTM) network, and deep neural network (DNN) to recognize six types of radar signals. This method does not need to convert the signals into images, which can effectively reduce the amount of computation, but it is less effective in recognizing continuous wave (CW) signals and binary phase shift keying (BPSK) signals, especially the CW signals. For the time–frequency domain, some time–frequency analysis (TFA) techniques are used to characterize signals in both time and frequency domains. Qin et al. [10] converted time-domain radar signals into time–frequency images (TFIs) and then used a residual network to identify modulation types of signals. Its overall recognition rate can reach more than 96% at −2-dB

Manuscript received 5 April 2023; revised 30 June 2023; accepted 19 July 2023. Date of publication 26 July 2023; date of current version 20 November 2023. This work was supported by the Key Research and Development Projects in Zhejiang Province under Grant 2022C01144. *(Corresponding author: Daying Quan.)*

The authors are with the Key Laboratory of Electromagnetic Wave Information Technology and Metrology, China Jiliang University, Hangzhou 310018, China (e-mail: qdy@cjlu.edu.cn).

Digital Object Identifier 10.1109/JMASS.2023.3299159

signal-to-noise ratio (SNR), but its performance degrades seriously with the decrease in SNR. Liu et al. [11] extracted features from the time–frequency domain and used an artificial bee colony algorithm-optimized support vector machine (SVM) as a classifier. When the SNR is −4 dB, its overall recognition rate can reach 92%. Yu and Tang [12] proposed a recognition method based on contour extraction, in which signal contour is used to replace the binary image and CNN is employed for signal recognition. Due to the advantages of small cross terms and strong anti-noise characteristics, the Choi–Williams distribution (CWD) is used to extract the time–frequency features of radar signals [10], [11], [12], [13]. But some signal details may be overlooked due to its low time–frequency resolution, which will affect the accuracy of recognition. To solve this problem, Oberlin et al. [14] proposed a synchronous squeeze transform (SST) based on the short-time Fourier transform (STFT) to "squeeze" signal frequency. Compared with the CWD transform, the TFI of SST has a higher resolution and can retain more details of signal features, which is beneficial to signal recognition. However, when SST processes complex time-variant signals, its time–frequency aggregation reduces greatly, resulting in the blurring of time–frequency features. As the signal nonstationarity increases, the error of the instantaneous frequency estimation increases too. Yu et al. [15] used multisynchrosqueezing transform (MSST) to perform time–frequency transformation on signals, which can alleviate the time–frequency feature ambiguity and energy divergence problems of synchrosqueezing. However, MSST is easily affected by noise under low SNR, which makes the radar signal easily distorted and affects the accuracy of identification.

In order to comprehensively exploit the different advantages of MSST and CWD and further improve the effectiveness of feature extraction, we construct a dual-channel feature extraction model, in which MSST and CWD are utilized individually to obtain different TFIs of radar signals, and the histogram of oriented gradients (HOG) algorithm is introduced to perform feature extraction. The HOG features extracted from the TFIs of the two channels are finally fused and dimensionally reduced for classification. The simulation experiments were taken on nine types of typical radar signals, including CW, different types of frequency modulation (FM), and phase modulation (PM) with the SNR range from −14 to 10 dB. The results show that the proposed approach achieves higher recognition accuracy than each single-channel scheme, and the advantage is more obvious under low SNR regions. The comparison with the other five models published in recent years also proves the validity of our dual-channel model.

The main contributions of this article are summarized as follows.

1) We present a radar signal recognition model based on the feature extraction of dual-channel TFIs. It improves the performance of radar signal recognition, especially in the low SNR scenario.
2) We take advantage of CWD's good anti-noise and MSST's high-resolution characteristics and extract more detailed features, which are beneficial to low SNR radar signal recognition.
3) Our model uses a simple SVM classifier for classification. The advantages of low computation complexity, few training samples, and less training time make it more suitable for engineering applications. Experiments on multipath fading channel environments demonstrate that our model has good stability and robustness.

TABLE I
MSST EXPRESSION

Compression times	Expression
Once	$T_s^{[1]}(t,\eta)=\int_{-\infty}^{+\infty} G(t,w)\delta(\eta-\hat{w}(t,w))dw$
Twice	$T_s^{[2]}(t,\eta)=\int_{-\infty}^{+\infty} T_s^{[1]}(t,w)\delta(\eta-\hat{w}(t,w))dw$
N times	$T_s^{[N]}(t,\eta)=\int_{-\infty}^{+\infty} T_s^{[N-1]}(t,w)\delta(\eta-\hat{w}(t,w))dw$

The subsequent sections of this article are structured in the following manner. In Section II, we discuss the radar signal processing algorithms, including MSST transform and CWD transform. Section III outlines the overall framework of the proposed method and provides a detailed explanation of image preprocessing, feature extraction, and feature dimensionality reduction. Section IV presents the experimental results and analysis. Finally, the conclusion is discussed in Section V.

II. TIME–FREQUENCY TRANSFORM

In this section, we provide a detailed explanation of the fundamental principles and procedures underlying the MSST and CWD transforms, which serve as the basis for the subsequent image preprocessing and feature extraction.

A. MSST Time–Frequency Transform

MSST is a new TFA method that can effectively enhance the resolution of the time–frequency distribution image by performing multiple simultaneous compression on the time–frequency spectrum obtained by STFT, and the iterative operators in MSST can use to optimize the algorithm process and reduce the computational burden. At the same time, as a linear time–frequency tool, MSST does not have the interference of cross terms. The expression of MSST is shown in Table I [15], where $T_s^{[N]}(t,\eta)$ is N-order synchronous compression, η is the output frequency, $G(t,w)$ is the STFT of the signal, $\hat{w}(t,w)$ is the instantaneous frequency estimation, and $\delta(t)$ is the impulse function. The first-order synchronous compression expression, i.e., SST, is obtained by compressing the STFT time–frequency distribution from the frequency direction. However, when SST compresses complex time-varying signals, the instantaneous frequency estimation deviation of the signal increases, and the time–frequency aggregation is greatly reduced, which will result in TFI blurring. But MSST can effectively handle strong modulation signals and strong time-varying signals by iterative calculation. At the same time, MSST also alleviates the problem of low time–frequency energy concentration of SST. The synchronous compression transformation is performed on $T_s^{[1]}(t,w)$ again to obtain the

double synchronous compression transformation $T_s^{[2]}(t, w)$. $T_s^{[N]}(t, w)$ is the output expression after N iterations.

B. CWD Time–Frequency Transform

CWD is a common Cohen class time–frequency distribution, which was proposed by Choi and Williams in 1989 [16]. By adding kernel function, time–frequency resolution and cross-term interference can be better balanced. The CWD time–frequency conversion formula is as follows [17]:

$$\mathrm{CWD}(t,f) = \iint \sqrt{\frac{\sigma}{4\pi\tau^2}} f(s,\tau) s\left(u+\frac{\tau}{2}\right) s^*\left(u-\frac{\tau}{2}\right) e^{-j2\pi f\tau} du d\tau \quad (1)$$

$$f(s,\tau) = \exp\left[-\frac{\sigma(s-t)^2}{4\tau^2}\right] \quad (2)$$

the parameter σ represents the attenuation factor, $f(s, \tau)$ represents the kernel function, $s(u)$ represents the independent variable, f represents the frequency, τ denotes autocorrelation, and t represents time.

Fig. 1 shows the MSST and CWD TFIs of nine typical radar signals. It can be seen that the MSST time–frequency diagram has a high time–frequency resolution, and the CWD time–frequency diagram has better signal location distribution information.

III. Recognition Model

Based on the time–frequency transformation in Section II, we propose a radar signal recognition approach using a dual-channel model with HOG feature extraction. First, we obtain the TFIs of radar signals using MSST and CWD, respectively. Second, HOG features are extracted from the preprocessed TFIs from the two channels and then merged to obtain combined HOG features. Afterward, we use principal component analysis (PCA) to fuse and reduce the dimensionality of the combined features. Finally, the SVM classifier is used to classify signals based on extracted features and achieve radar signal identification. The flowchart of the system is shown in Fig. 2.

The recognition algorithm can be broadly divided into three key parts: 1) TFI preprocessing; 2) HOG feature extraction; and 3) PCA dimensionality reduction and recognition, as illustrated in Fig. 2. In this section, we provide a detailed account of these parts.

A. Time–Frequency Image Preprocessing

With the rapid development of electromagnetic equipment, the electromagnetic signals on the battlefield have become increasingly complex, and the signals generated by various electromagnetic devices will cause noise interference to the receiver. Although time–frequency conversion of radar signals can effectively reduce noise interference, there is still a substantial amount of interference information in images. Therefore, preprocessing of the TFI is necessary before feature extraction. We utilize grayscale, filtering, interpolation, and binarization to denoise TFIs. Fig. 3 shows the schematic of the preprocessing process and the TFI transformation.

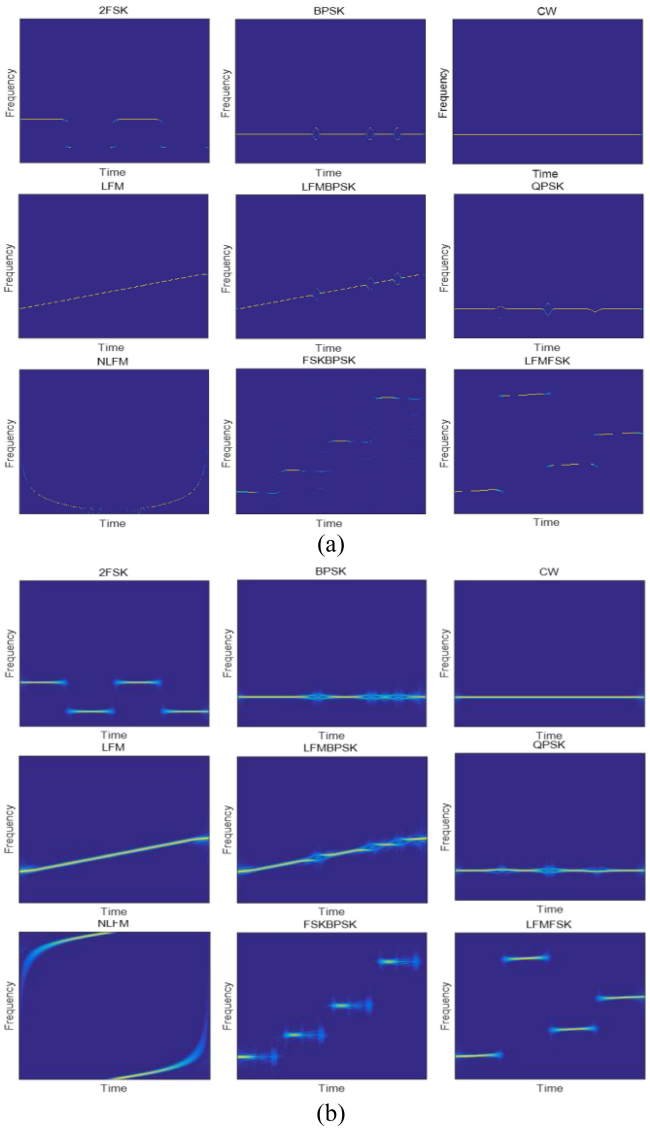

Fig. 1. TFIs. (a) MSST TFIs. (b) CWD TFIs.

The preprocessing of the TFI can be described as follows.

1) Perform grayscale processing to obtain grayscale images.
2) Subsequently, the Wiener filter is used to reduce the noise interference in gray images.
3) Finally, bicubic interpolation and binarization [18] are employed to decrease image noise and computational complexity, and thus an image of 224 × 224 pixels is obtained.

B. HOG Feature Extraction

The HOG operator describes the local texture features of objects by calculating the gradient value and gradient direction of pixels in the image and constructs the histogram with the obtained gradient value and gradient direction [19]. The HOG feature parameters are composed of the amplitude values in the histogram. Since the gradient information in the

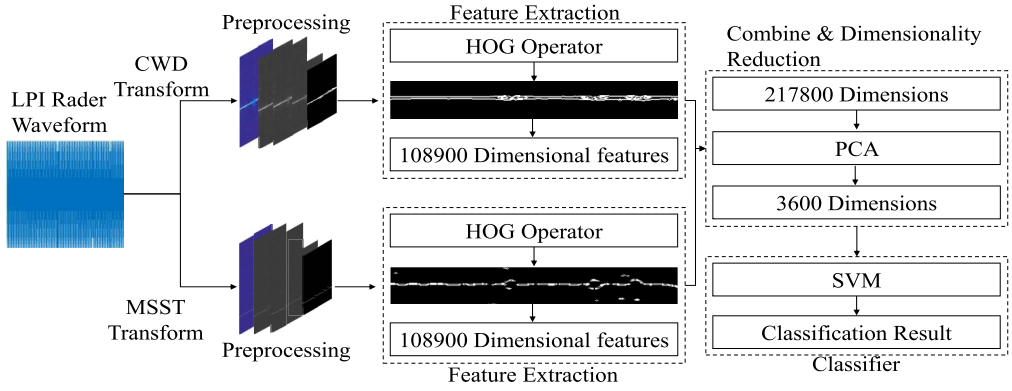

Fig. 2. Overall flowchart of the system.

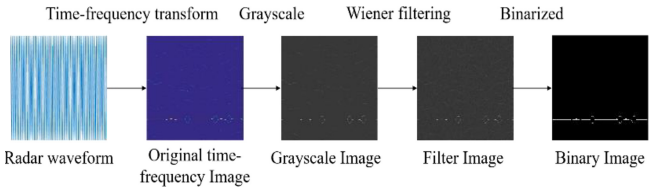

Fig. 3. Image preprocessing flowchart.

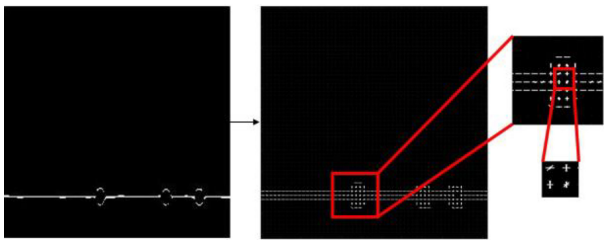

Fig. 4. HOG feature visualization.

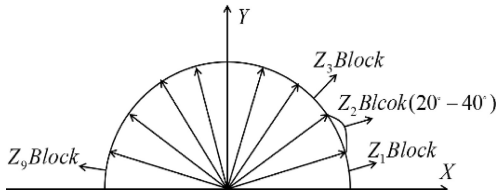

Fig. 5. Gradient direction block.

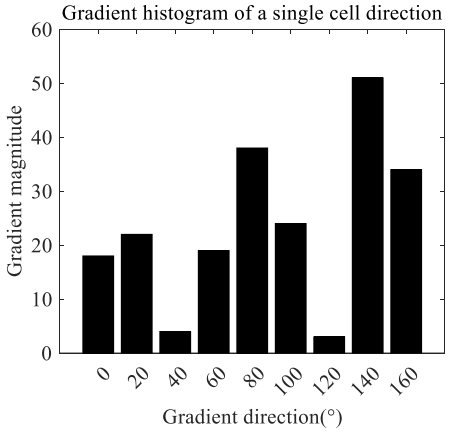

Fig. 6. Orientation gradient histogram.

image is mainly located in the edge area of the object, the HOG operator can describe the contour of the signal in the image by calculating the gradient information of the signal, as shown in Fig. 4. Inspired by this idea, we apply HOG feature extraction to realize edge and shape detection in the time–frequency domain. Moreover, the time–frequency aggregation of the signal is enhanced by the time–frequency transformation in Section II-A and binarization described in Section III-A, which makes the signal contour more obvious and facilitates the extraction of effective gradient values as feature parameters by the HOG operator. The specific derivation process is as follows.

1) Gradient Calculation: Gradient mainly includes gradient value and gradient direction. $G_x(x, y)$ and $G_y(x, y)$ in (3) and (4) represent the components of gradient value on the x-axis and y-axis, and (5) and (6) are the calculation process of gradient magnitude and gradient direction. $H(x, y)$ is the pixel value

$$G_x(x, y) = H(x + 1, y) - H(x - 1, y) \tag{3}$$

$$G_y(x, y) = H(x, y + 1) - H(x, y - 1) \tag{4}$$

$$G(x, y) = \sqrt{G_x(x, y)^2 + G_y(x, y)^2} \tag{5}$$

$$\alpha(x, y) = \tan^{-1}\left(\frac{G_y(x, y)}{G_x(x, y)}\right). \tag{6}$$

2) Gradient Direction Histogram Construction: According to Fig. 5, the gradient direction can be divided into nine angular regions. Meanwhile, the abscissa of the histogram in Fig. 6 is set according to the angular region divided. Then, the gradient value and gradient direction obtained from (5) and (6) are mapped to nine angular regions. Taking Tables II and III as examples, the gradient direction and gradient value in the table are mapped to the histogram. The nine amplitudes of the histogram are ultimately tallied as the 9-D feature vector of the corresponding cell [20].

The image pixel size is 224 × 224 and the cell size is 4 × 4, so there are 56 cells in each row of the image. The block is a square composed of four cells. Feature extraction is performed by moving the block on the image, and the moving step is 1, then an image needs to be moved $(224/4 - 1) \times (224/4 - 1)$

TABLE II
GRADIENT DIRECTION

Gradient direction value			
90	150	80	70
10	105	140	30

TABLE III
GRADIENT VALUE

The gradient value			
30	68	4	38
36	12	17	8

times in total, i.e., it needs to be moved 55 × 55 times. So we can get 4 × 9 × 55 × 55 = 108 900-D features from one image.

C. PCA Dimension Reduction

In this article, we extract the HOG features from dual-channel TFIs and then combine the two-channel features to obtain 217 800-D features. However, the merged features contain a significant amount of redundant information resulting from its high dimensions, which will reduce the classification speed and recognition accuracy. Therefore, the PCA algorithm is employed to reduce the dimension of the merged features, which can be formulated as

$$Y_{\mathrm{PCA}} = W^T Z_{\mathrm{HOG}} \tag{7}$$

where Z_{HOG} represents the fused HOG feature vector, and Y_{PCA} represents the feature vector after dimension reduction, W is the covariance matrix. Through the application of PCA dimensionality reduction, the HOG features are effectively compressed from an initial 108 900 dimensions down to 3600 dimensions.

Based on the detailed descriptions of the three sections above, we can summarize the recognition steps as follows.

1) Perform TFA and preprocessing on the time-domain signals to obtain binary images of MSST and CWD with a size of 224 × 224.
2) Then, HOG feature extraction is conducted on the two channels separately to obtain features with a dimensionality of 108 900 for each channel.
3) Finally, the features from the two channels are fused and dimensionally reduced by PCA to obtain 3600-D features for SVM model recognition.

IV. EXPERIMENTAL RESULTS AND ANALYSIS

To verify that the above recognition system has a good recognition rate and recognition speed, in this section, we carry out simulation experiments from four aspects: 1) TFIs comparison; 2) algorithmic comparison; 3) ablation experiment; and 4) robustness analysis. The computer hardware conditions of the simulation experiment are: Intel Core i7-10875H, GPU: NVIDIA GeForce RTX 1650, and the simulation tool is MATLAB. We also simulated a complex channel experiment for testing and recognized radar signals after Rayleigh fading to verify the effectiveness of the algorithm.

TABLE IV
WAVEFORM PARAMETERS

Radar Waveform	Simulation Parameter	(f_s =200MHz)
2FSK	Fundamental frequency f_h	f_1 , f_2 =10,30MHz
BPSK	Barker codes N_c	7
	Carrier frequency f_c	20MHz
CW	Carrier frequency f_c	20MHz
LFM	Initial frequency f_0	20MHz
	Bandwidth B	15MHz
NLFM	Initial frequency f_0	20MHz
	Bandwidth B	15MHz
QPSK	Carrier frequency f_c	20MHz

A. Dataset Design

In this article, nine typical radar signals, including CW, LFM, BPSK, QPSK, 2FSK, NLFM, LFM/BPSK, LFM/FSK, and FSK/BPSK, are selected for experiments. The radar signal parameters are set as Table IV.

The composite modulation parameter settings are consistent with the above. The experiments are conducted in a Gaussian white noise environment, the SNR of the signals is set from −14 to 10 dB, and the step size is 2 dB. The sample number of each signal is 600. The training set size is 400, and the test set size is 200.

B. Time–Frequency Image Comparison

Fig. 7 shows four time–frequency transformations of the BPSK signal: WVD, SST, CWD, and MSST. From Fig. 7, we can see that CWD transform and MSST transform have the best signal characteristics and resolution, respectively.

To further verify the performance of the four transformations, we carried out signal recognition experiments for the four kinds of TFIs. The simulation parameters are set according to Section IV-A. The experimental result in Fig. 8 shows that the recognition rate of the MSST transform and CWD transform is higher than the other two time–frequency transforms, as we expected.

C. Algorithm Comparison Experiment

1) Algorithm Recognition Accuracy Comparison: To verify the high recognition rate by combining CWD and MSST, we design three sets of comparative experiments.

Fig. 9 shows the comparison of the recognition accuracy combining different TFIs. From the figure, we can conclude that the dual channel of MSST and CWD has the best recognition rate. Since the CWD TFI and the MSST TFI are better at distinguishing PM signals and FM signals, the combination of these two TFIs can enhance the recognition of radar signals. Besides, under the condition of low SNR, the recognition accuracy of the combination of CWD and WVD is higher than that of the combination of MSST and WVD, but it is the opposite when the SNR is more than −10 dB. The above conclusions confirm the analysis in Section IV-D, i.e., the CWD TFI has

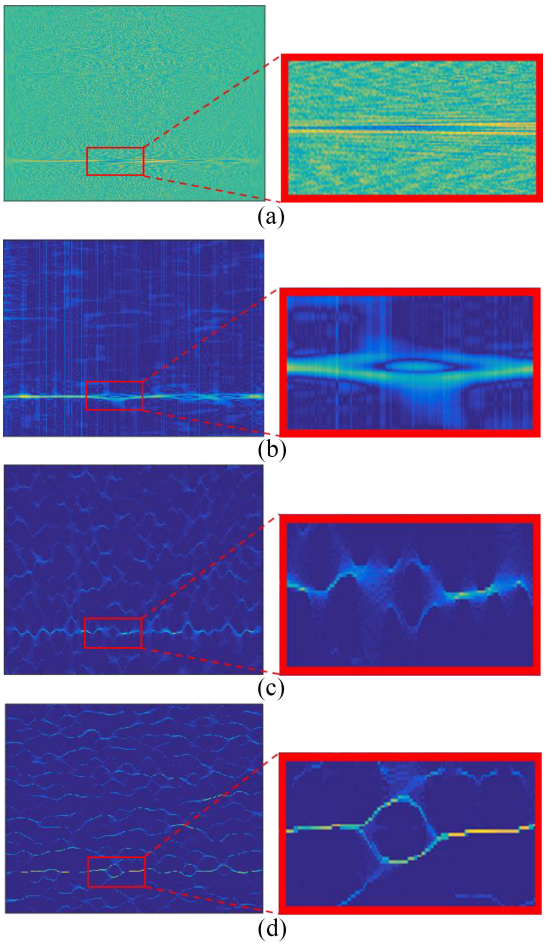

Fig. 7. Four kinds of TFIs. (a) WVD images. (b) CWD images. (c) SST images. (d) MSST images.

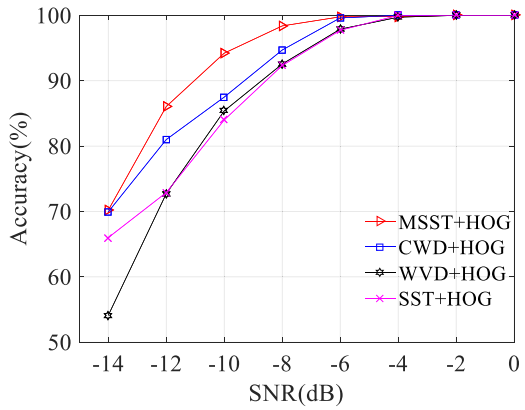

Fig. 8. Accuracy comparison of four TFIs.

good noise resistance under low SNR, while the MSST can better represent the contour characteristics of the signal.

We also consider combining multiple (more than two) time–frequency transformation methods, and the accuracy comparison is shown in Fig. 10. It can be seen that the combination of four time–frequency transformations (MSST, CWD, SST, and WVD) brings the highest recognition accuracy, and the combination of the three time–frequency transformations also improves the accuracy under some SNRs. It demonstrates that

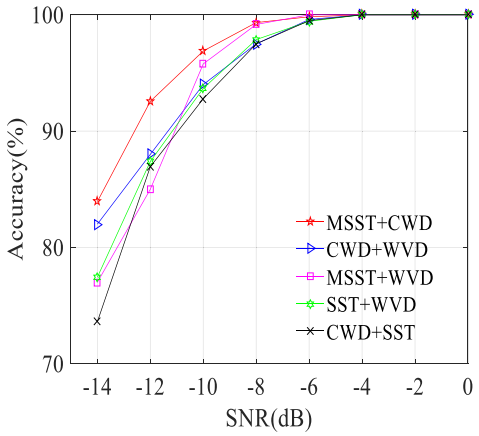

Fig. 9. Different dual-channel recognition accuracy diagram.

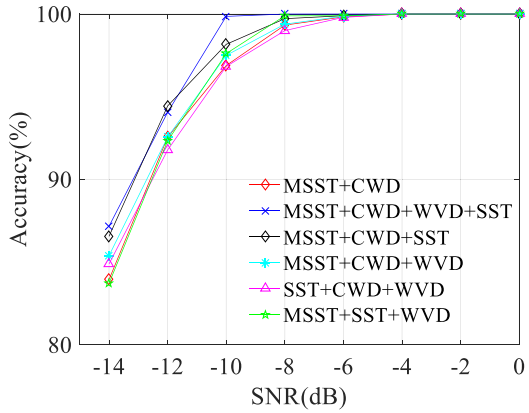

Fig. 10. Accuracy comparison of various time–frequency transform combinations.

TABLE V
ALGORITHM TRAINING TIME

Method	Number	SNR(dB)/Time(s)			
		-14	-12	-10	-8
MSST+CWD	7200	138	132	122	114
MSST+CWD+SST+WVD	14400	461	458	453	448
MSST+CWD+SST	10800	377	372	365	358
MSST+CWD+WVD	10800	353	345	337	342
MSST+SST+WVD	10800	324	321	320	314
CWD+SST+WVD	10800	395	349	319	282

combining multiple time–frequency transformation methods brings better recognition performance. However, combining more time–frequency transformation methods typically results in higher computational complexity. Table V shows the computational cost of various time–frequency transformation combinations. It can be seen that the proposed method requires less training time but achieves higher recognition accuracy. When the SNR is −12 dB, the recognition accuracy of the proposed method is higher than other three time–frequency transform combinations.

Moreover, we also compare our model with two traditional machine learning models (Meng et al. [21] and Li et al. [22]), and three CNN-based models [23], [24], [25]. The experimental results are shown in Fig. 11.

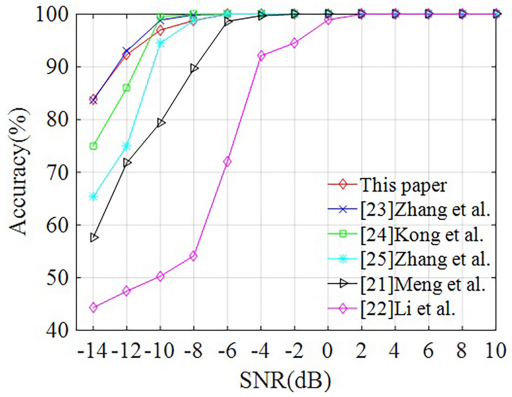

Fig. 11. Average recognition rates of the five algorithms are compared.

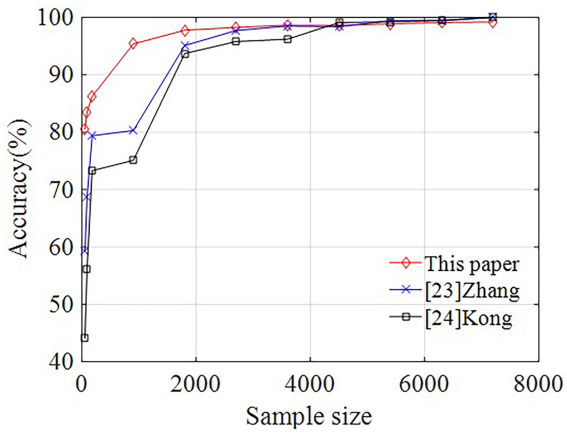

Fig. 12. Comparison of recognition accuracy with different sizes of the training set.

With the decrease of the SNR, the radar signal is gradually covered by noise, resulting in a decrease in frequency image quality. As shown in Fig. 11, the LBPV features used in [21] cannot extract the texture features of the images well at low SNR, which leads to a serious decrease in accuracy. When the SNR is below −10 dB, the recognition accuracy of the LBPV algorithm is less than 80%. However, the two-channel model proposed in this article has better frequency aggregation and more effective features can be extracted from the images. Also, the features extracted by the HOG operator can describe the signal more completely and have better noise immunity. Therefore, when the SNR is −12 dB, the accuracy reaches 92.5%, and the algorithm can still maintain a high recognition rate even at a lower SNR. Literature [22] also used two-channel TFIs, but there is no complementarity between the two TFIs, and the quality of AF TFIs decreases sharply as the SNR decreases, which leads to a serious decrease in recognition accuracy at low SNR, while the feature dimensionality extracted by GLGCM is less and cannot reflect the signal characteristics well. The dual channel used in this article can better distinguish the FM signal and the PM signal, and the feature dimension extracted by the HOG operator is high, which can reflect the characteristics of the signal more comprehensively. At the same time, to reduce the dimensionality and redundant features, we use PCA for dimensionality reduction.

Compared with [23] and [24], the recognition rate of this article is slightly higher at low SNR. When the SNR is greater than −12 dB, the recognition rate of this article is slightly lower than [23] and [24], but from Fig. 12, we can know that when the number of training set is small, the recognition accuracy of the CNN model will be lower than our method. When the SNR is −8 dB, the recognition accuracy of the three models is close to 100%. Literature [25] has the lowest recognition rate among these three CNN-based models. This is because it has only two convolutional layers and the model structure is simple. In the low SNR, the accuracy of the dual-channel algorithm identification used in this article is much higher than that of [25].

2) Comparison of Recognition Accuracy With Different Sizes of the Training Set: Compared with deep learning, SVM has the advantages of low complexity and fewer sample requirements. It can be seen from Fig. 12 that when the number of samples is less than 1000, the SVM-based recognition accuracy of this article is much higher than the other two CNN-based recognition methods, and SVM has obvious advantages in small sample classification.

D. Ablation Experiment

Fig. 13 shows the confusion matrix for recognizing nine signals when the SNR is −14 dB. The numbers in the confusion matrix represent the recognition rate, where the recognition rate on the diagonal represents the correct recognition rate of the nine signals, and the remaining recognition rates represent the recognition accuracy of signals incorrectly recognized as other signals. Through the confusion matrix, we can not only determine the recognition accuracy of the signals but also identify which signals are more likely to be confused with each other, which is beneficial for analyzing the characteristics of the signals. From the confusion matrix in Fig. 13, we observe that MSST time–frequency transform has a higher recognition rate for phase-modulated signals, like QPSK, while CWD time–frequency transform has a higher recognition rate for frequency-modulated signals, such as 2FSK, FSK/LFM, and FSK/BPSK. Because the MSST transform has a high time–frequency aggregation degree and no cross terms, the signal contour is obvious. Even in the hopping phase of the phase-modulated signal, there is still a good frequency aggregation degree, which is conducive for the HOG operator to extract the signal contour gradient as the feature vector. But at low SNR, the instantaneous frequency is also affected by noise, resulting in signal distortion in the TFI, as shown in Fig. 14(a). The CWD transform has good noise resistance, and the signal in the TFI is not easily distorted under lower SNR, so the recognition rate of the frequency-modulated signal is high. However, the CWD TFIs have signal blurring and cross terms in phase hopping, which are easily confused with other phase-modulated signals, resulting in a low recognition rate of phase-modulated signals, as shown in Fig. 14(b).

To gain the benefits of MSST and CWD images, we combine the features extracted from the two TFIs to form a dual-channel confusion matrix shown in Fig. 13(c). From the figure, we can see that the combined recognition accuracy is greatly improved. The recognition rates of frequency-modulated

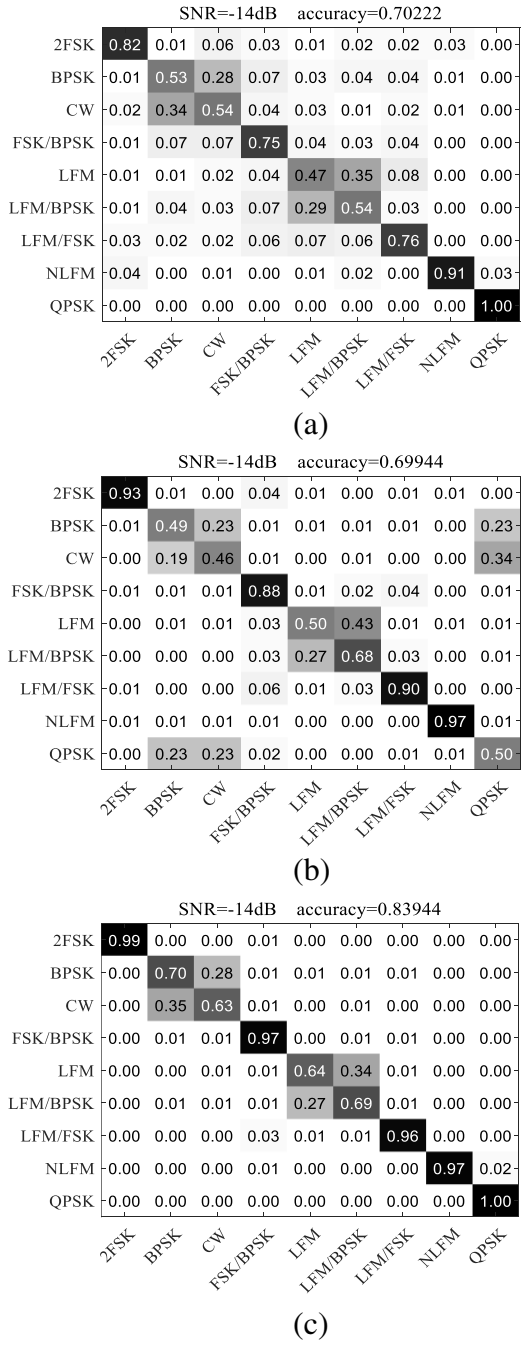

Fig. 13. Confusion matrix comparison diagram. (a) Confusion matrix for MSST. (b) Confusion matrix for CWD. (c) Confusion matrix for dual channel.

signals and mixed modulation with frequency-modulated signals are higher than 95%, and the recognition rates of phase-modulation signals are also improved by about 15%.

As shown in Fig. 15, when the SNR is lower than −8 dB, the accuracy of the dual-channel model is superior to the single-channel TFI model. Especially when the SNR is −14 dB, the accuracy of the dual-channel model is 13% higher than the single-channel model. When the SNR is higher than −8 dB, the recognition accuracy of the three models approaches 100%. From the above analysis, it can be concluded that the dual-channel TFI model has better performance in the region of low SNR.

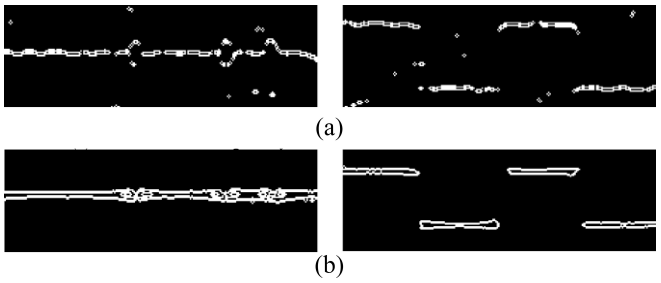

Fig. 14. Signal contour image. (a) MSST TFIs of 2FSK and BPSK. (b) CWD TFIs of 2FSK and BPSK.

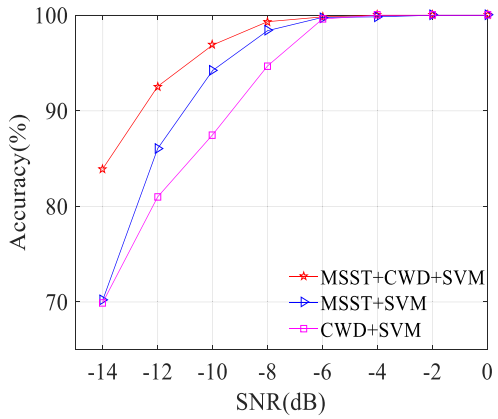

Fig. 15. Dual-channel comparison diagram.

TABLE VI
OVERALL RECOGNITION RATE OF THE TRAINING SET AND TEST SET UNDER DIFFERENT SNRS

Training set (SNR/dB)	Test set (SNR/dB)	Recognition rate
-14	-8	0.9406
-4	0	1
0	-2	0.9022
-14~10	-14~10	0.9202

E. Robustness Experiment

To test the robustness of the proposed model, we test the model with different SNRs. The measured data are shown in Table VI.

As shown in Table VI, the recognition rate under different SNRs or mixed SNRs is above 90%, which proves that the model in this article has a good recognition rate and robustness.

F. Multipath Fading Channels

In order to make the simulated radar signals closer to the real electromagnetic scenario, we add multipath fading to simulate the real scenario. Fig. 16 simulates the process of radar signal transmission in a realistic scenario. The data set contains nine kinds of signals, and the waveform parameters and channel conditions are summarized in Tables VII and VIII. The parameters of the composite modulation signal are set according to the single signal parameters [26].

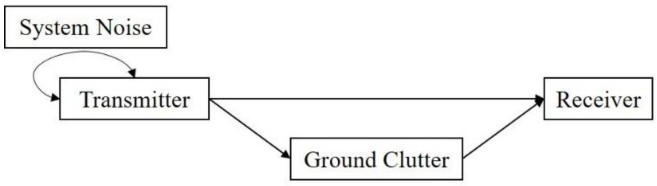

Fig. 16. Multipath fading model.

TABLE VII
WAVEFORM PARAMETERS UNDER MULTIPATH FADING CHANNELS

Radar Waveform	Simulation Parameter	(f_s =200MHz)
2FSK	Fundamental frequency f_h	$U(1/80,1/2)$
BPSK	Barker codes N_c	{7,11,13}
	Carrier frequency f_c	$U(1/8,1/4)$
CW	Carrier frequency f_c	$U(1/8,1/4)$
LFM	Initial frequency f_0	$U(1/16,1/8)$
	Bandwidth B	$U(1/16,1/8)$
NLFM	Initial frequency f_0	$U(1/16,1/8)$
	Bandwidth B	$U(1/16,1/8)$
QPSK	Carrier frequency f_c	$U(1/8,1/4)$

TABLE VIII
CHANNEL CONFIGURATION

Model	Rayleigh
ψ	$U(1,1000)$ ns
G	$U(-14,0)$ dB
$f_{D\max}$	$U(10,1000)$ Hz

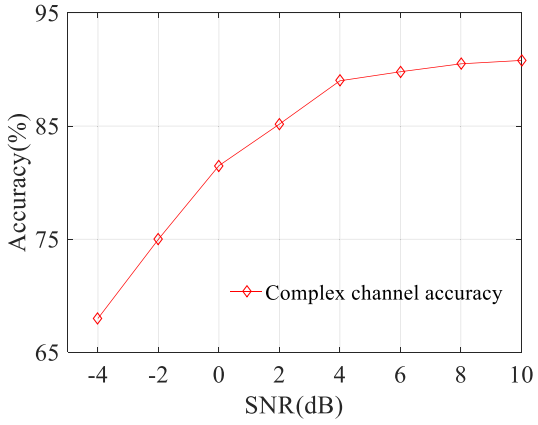

Fig. 17. Complex channel accuracy.

From the graph in Fig. 17, it can be seen that it is difficult to recognize radar signals in the complex channel because the signal is severely damaged by path delay and path gain, and a large amount of texture information on the TFI is lost. At the same time, the Doppler frequency shift changes the frequency and phase of the signal, making it more difficult to distinguish the complex modulated signal from other signals. However, the method in this article can still maintain more than 80% recognition accuracy when the SNR is higher than 0 dB and can reach more than 90% when the SNR is 10 dB.

V. CONCLUSION

In this work, we propose a novel method for radar signal recognition using a dual-channel model and HOG feature extraction. This method combines the characteristics of CWD's good noise immunity and MSST's high time–frequency aggregation and can better distinguish frequency-modulated signals from phase-modulated signals. Moreover, the signal contour after multiple simultaneous compression is more obvious, which is beneficial for the HOG operator to extract edge gradient information as an effective feature. The addition of the PCA dimensionality reduction method reduces redundant features and computational complexity. Finally, SVM is used for effective identification. According to the experimental simulation results, this method has a good recognition effect under low SNR, especially for FM signals and PM signals. We can also find that the dual-channel model combined with MSST and CWD achieves higher recognition accuracy than single-channel models. The proposed method effectively alleviates the difficulty of effective feature extraction under low SNR by extracting signal features of different TFIs and provides a new scheme for radar signal recognition in electronic reconnaissance.

ACKNOWLEDGMENT

The authors thank the Editor for reading this article carefully and for providing valuable comments, which have improved the presentation of this article.

REFERENCES

[1] Y. Luo, M. Xu, Z. Wu, and Z. Yin, "Signal detection and modulation recognition based on convolutional neural networks," in *Proc. IEEE Int. Conf. Artif. Intell. Comput. Appl. (ICAICA)*, 2022, pp. 295–299.
[2] V. Iglesias, J. Grajal, P. Royer, M. A. Sanchez, M. Lopez-Vallejo, and O. A. Yeste-Ojeda, "Real-time low-complexity automatic modulation classifier for pulsed radar signals," *IEEE Trans. Aerosp. Electron. Syst.*, vol. 51, no. 1, pp. 108–126, Jan. 2015.
[3] D. C. Schleher, "LPI radar: Fact or fiction," *IEEE Aerosp. Electron. Syst. Mag.*, vol. 21, no. 5, pp. 3–6, May 2006.
[4] Y. Huang, W. Jin, P. Ge, and B. Li, "Radar emitter signal identification based on multi-scale information entropy," *J. Electron. Inf. Technol.*, vol. 41, no. 5, pp. 1084–1091, 2019.
[5] J. B. Tsui, *Digital Techniques for Wideband Receivers*. Stevenage, U.K.: SciTech Publ., 2004.
[6] J. Lunden and V. Koivunen, "Automatic radar waveform recognition," *IEEE J. Sel. Topics Signal Process.*, vol. 1, no. 1, pp. 124–136, Jun. 2007.
[7] R. Mingqiu, C. Jinyan, Z. Yuanqing, and H. Jun, "Radar signal feature extraction based on wavelet ridge and high order spectral analysis," in *Proc. IET Int. Radar Conf.*, 2009, pp. 1–6.
[8] C. Wang, H. Gao, and X. Zhang, "Radar signal classification based on auto-correlation function and directed graphical model," in *Proc. IEEE Int. Conf. Signal Process. Commun. Comput. (ICSPCC)*, 2016, pp. 1–4.
[9] S. Wei, Q. Qu, H. Su, M. Wang, J. Shi, and X. Hao, "Intra-pulse modulation radar signal recognition based on CLDN network," *IET Radar, Sonar Navig.*, vol. 14, no. 6, pp. 803–810, 2020.
[10] X. Qin, X. Zha, J. Huang, and L. Luo, "Radar waveform recognition based on deep residual network," in *Proc. IEEE 8th Joint Int. Inf. Technol. Artif. Intell. Conf. (ITAIC)*, 2019, pp. 892–896.

[11] L. Liu, S. Wang, and Z. Zhao, "Radar waveform recognition based on time-frequency analysis and artificial bee colony-support vector machine," *Electronics*, vol. 7, no. 5, p. 59, 2018.
[12] Z. Yu and J. Tang, "Radar signal intra-pulse modulation recognition based on contour extraction," in *Proc. IEEE Int. Geosci. Remote*, 2020, pp. 2783–2786.
[13] S. G. Bhatti and A. I. Bhatti, "Radar signal intrapulse modulation recognition using phase-based STFT and BiLSTM," *IEEE Access*, vol. 10, pp. 80184–80194, 2022.
[14] T. Oberlin, S. Meignen, and V. Perrier, "The fourier-based synchrosqueezing transform," in *Proc. IEEE Int. Conf. Acoust., Speech Signal Process.*, 2014, pp. 315–319.
[15] G. Yu, Z. Wang, and P. Zhao, "Multisynchrosqueezing transform," *IEEE Trans. Ind. Electron.*, vol. 66, no. 7, pp. 5441–5455, Jul. 2019.
[16] H.-I. Choi and W. J. Williams, "Improved time-frequency representation of multicomponent signals using exponential kernels," *IEEE Trans. Acoust., Speech, Signal Process.*, vol. 37, no. 6, pp. 862–871, Jun. 1989.
[17] D. Quan, Z. Tang, X. Wang, W. Zhai, and C. Qu, "LPI radar signal recognition based on dual-channel CNN and feature fusion," *Symmetry*, vol. 14, no. 3, p. 570, 2022.
[18] R. Ataie, A. A. E. Zarandi, and Y. S. Mehrabani, "An efficient inexact full adder cell design in CNFET technology with high-PSNR for image processing," *Int. J. Electron.*, vol. 106, no. 6, pp. 928–944, 2019.
[19] S. Zhang and X. Wang, "Human detection and object tracking based on histograms of oriented gradients," in *Proc. 9th Int. Conf. Nat. Comput. (ICNC)*, Shenyang, China, Jul. 2013, pp. 1–6.
[20] S. A. Korkmaz, A. Akçek, H. Bínol, and M. F. Korkmaz, "Recognition of the stomach cancer images with probabilistic HOG feature vector histograms by using HOG features," in *Proc. IEEE 15th Int. Symp. Intell. Syst. Inform. (SISY)*, Sep. 2017, pp. 339–342.
[21] M. Fanjie, T. Hong, W. Yizhe, and L. Junjie, "Radar emitter signal recognition based on time-frequency image texture feature," *J. Projectiles, Missiles Guid.*, vol. 37, no. 3, pp. 152–156, 2017.
[22] S. Li, D. Quan, X. Wang, and X. Jin, "LPI radar signal modulation recognition with feature fusion based on time-frequency transforms," in *Proc. 13th Int. Conf. Wireless Commun. Signal Process. (WCSP)*, 2021, pp. 1–6.
[23] M. Zhang, M. Diao, and L. Guo, "Convolutional neural networks for automatic cognitive radio waveform recognition," *IEEE Access*, vol. 5, pp. 11074–11082, 2017.
[24] S.-H. Kong, M. Kim, L. M. Hoang, and E. Kim, "Automatic LPI radar waveform recognition using CNN," *IEEE Access*, vol. 6, pp. 4207–4219, 2018.
[25] J. Zhang, Y. Li, and J. Yin, "Modulation classification method for frequency modulation signals based on the time–frequency distribution and CNN," *IET Radar, Sonar Navig.*, vol. 12, no. 2, pp. 244–249, 2018.
[26] T. Huynh-The, V.-S. Doan, C.-H. Hua, Q.-V. Pham, T.-V. Nguyen, and D.-S. Kim, "Accurate LPI radar waveform recognition with CWD-TFA for deep convolutional network," *IEEE Wireless Commun. Lett.*, vol. 10, no. 8, pp. 1638–1642, Aug. 2021.